Revista Mexicana de Astronomía y Astrofísica, **50**, 307–322 (2014)

FOURIER DECOMPOSITION OF RR LYRAE LIGHT CURVES AND THE SX PHE POPULATION IN THE CENTRAL REGION OF NGC 3201

A. Arellano Ferro,[1,2] J. A. Ahumada,[3] J. H. Calderón,[1,3,4] and N. Kains[5]

Received April 23 2014; accepted June 10 2014

RESUMEN

Presentamos el análisis de una serie temporal de imágenes CCD de la región central del cúmulo globular NGC 3201. El objetivo principal de este trabajo es la descomposición de Fourier de las curvas de luz de las estrellas RR Lyrae y su empleo en la determinación de la metalicidad del cúmulo y de su distancia. De esta manera hemos obtenido, para la metalicidad, el valor medio $[\mathrm{Fe/H}]_{ZW} = -1.483 \pm 0.006$ (estadístico) ± 0.090 (sistemático), y para la distancia, 5.000 ± 0.001 kpc (estadístico) ± 0.220 (sistemático). La metalicidad y la distancia estimados a partir de dos estrellas RRc son congruentes con los anteriores. Debido a la presencia de enrojecimiento diferencial, derivamos valores individuales de $E(B-V)$ para las estrellas RR Lyrae analizando sus curvas de color $V-I$. El valor promedio encontrado es $E(B-V) = 0.23 \pm 0.02$. Una exploración de las curvas de luz de las estrellas en la región de las *blue stragglers* condujo al descubrimiento de tres nuevas variables SX Phe. La relación periodo-luminosidad de las estrellas SX Phe se empleó para obtener una determinación independiente de la distancia al cúmulo y de los enrojecimientos individuales. La distancia calculada fue de 5.0 kpc.

ABSTRACT

CCD time-series observations of the central region of the globular cluster NGC 3201 were obtained with the aim of performing the Fourier decomposition of the light curves of the RR Lyrae stars present in that field. This procedure gave the mean values, for the metallicity, of $[\mathrm{Fe/H}]_{ZW} = -1.483 \pm 0.006$ (statistical) ± 0.090 (systematic), and for the distance, 5.000 ± 0.001 kpc (statistical) ± 0.220 (systematic). The values found from two RRc stars are consistent with those derived previously. The differential reddening of the cluster was investigated and individual reddenings for the RR Lyrae stars were estimated from their $V-I$ curves. We found an average value of $E(B-V) = 0.23 \pm 0.02$. An investigation of the light curves of stars in the *blue straggler* region led to the discovery of three new SX Phe stars. The period-luminosity relation of the SX Phe stars was used for an independent determination of the distance to the cluster and of the individual reddenings. We found a distance of 5.0 kpc.

Key Words: globular clusters: individual: (NGC 3201) — stars: variables: RR Lyrae

1. INTRODUCTION

NGC 3201 (C1015−461 in the IAU nomenclature) is a nearby (∼4.9 kpc) and very extended globular cluster with a very sparse central region. These characteristics have contributed to make it the subject of intensive and successful searches for variable stars over the past one hundred years. Despite its proximity, the cluster has considerable differential reddening (e.g., von Braun & Mateo 2001; Piotto et al. 2002; Layden & Sarajedini 2003), which is not unexpected given its position near the Galactic plane ($l = 277.23^{\circ}$, $b = +8.64^{\circ}$). It is rich in variable stars; the 2012 update to the Catalogue of Variable Stars in Globular Clusters (CVSGC, Clement et al. 2001) lists 121 variables contained approximately within half a square degree around the cluster center, among them: 86 RR Lyrae stars, 13 SX Phoenicis, 8 long period variables, 3 eclipsing binaries, and 11 non-variables previously

[1]Visiting Astronomer, Complejo Astronómico El Leoncito, operated under agreement between the Consejo Nacional de Investigaciones Científicas y Técnicas de la República Argentina, and the National Universities of La Plata, Córdoba, and San Juan, Argentina.

[2]Instituto de Astronomía, Universidad Nacional Autónoma de México, Mexico.

[3]Observatorio Astronómico, Universidad Nacional de Córdoba, Córdoba, Argentina.

[4]Consejo Nacional de Investigaciones Científicas y Técnicas, Argentina.

[5]Space Telescope Science Institute, Baltimore, USA.

suspected of variability. The first 56 variables in the cluster were found by Woods (1919) on a few Harvard plates obtained in 1916 at the Boyden Station of Harvard Observatory near Arequipa, Peru. A few variables, now numbered V57–V61, were added by Bailey (1922) from deep-exposure (2- and 4-hour) plates also at Arequipa. Continuing these efforts, Dowse (1940) announced the discovery of 25 more variables, V62–V86, on 60 new plates. Star V87 was discovered by Wright (1941) during an investigation of variable star periodicities, also on Arequipian plates. No further variable search was undertaken until 24 years later when Wilkens (1965) discovered variables V88–V96. Up to then, the large majority of variables were of the RRab type, four were RRc, and a few others would turn out to be non-variable in later, more precise, studies. Stars V97–V100 were found from photometric and photographic data by Lee (1977). More than twenty years later, already in the CCD era, von Braun & Mateo (2002) found the eclipsing binary V101 and other short-period variables in the field of the cluster, mostly eclipsing binaries and one RR Lyrae which they argued were not cluster members. The first group of SX Phe stars, V102–V112, was identified by Mazur et al. (2003). Layden & Sarajedini (2003) (LS03) detected low-light variations in some bright red giants (V113–V118), and discovered another eclipsing binary (V119) and two probable SX Phe stars (V120 and V121).

The present investigation is the first one that uses the difference image analysis (DIA) technique on NGC 3201. The virtues of DIA as a powerful tool to discover short-period variable stars, or unveil small amplitude variations in Blazhko RR Lyrae stars in the densely populated central regions of globular clusters, have been shown in several papers in the recent literature (e.g. Arellano Ferro et al. 2013a, 2012; Bramich et al. 2011; Figuera Jaimes et al. 2013; Kains et al. 2013, 2012, and references therein). We applied this method to the central regions of NGC 3201 on a set of data obtained under average-to-mediocre seeing conditions; in spite of this, our photometry led to clean light curves for the great majority of the RR Lyrae stars and allowed the discovery of three new SX Phe variables, as shall be described later.

The principal aim of the present paper is to offer a new time-series V and I CCD photometry that allows the refining of the periods of the variables as well as the Fourier decomposition of the light curves of the RR Lyrae population to estimate its iron content [Fe/H] and distance independently; we also want to compare the cluster distance obtained via the SX Phe period-luminosity (P-L) relation to estimates derived with other methods. In the process we shall discuss the peculiarities of several stars of the cluster population of variables.

The layout of the paper is as follows: In § 2 we describe the observations, data reductions, and transformation of our photometry to the standard system. In § 3 the distribution of the variable stars in the color-magnitude diagram (CMD) is presented and the discovery of three new SX Phe stars is announced. The RR Lyrae are identified, their periods are refined, and their light curves are presented. In § 4 the individual reddenings of RR Lyrae stars are calculated and the Fourier decomposition of their light curves is performed to estimate their metallicity, luminosity, mass, and radius. The distribution of the RR Lyrae stars on the Bailey diagram (amplitude versus period) is discussed. In § 5 we address the P-L relation for SX Phe stars and comment on the implied cluster distance. § 6 summarizes our results.

2. OBSERVATIONS AND REDUCTIONS

2.1. *Observations*

The Johnson-Kron-Cousins V and I observations used in the present work were obtained on March 19–22, 2013, with the 2.15-m telescope of the Complejo Astronómico El Leoncito (CASLEO), San Juan, Argentina. The estimated seeing varied between ≈ 1.5 and 2.8 arcsec, with a tendency to increase as each night progressed. The detector was a Roper Scientific back-illuminated CCD of 2048×2048 pixels with a scale of 0.15 arcsec/pix and a field of view (FoV) of approximately 5.1×5.1 arcmin^2. Our data consist of 143 V and 146 I images.

2.2. *Difference Image Analysis (DIA)*

Image data were calibrated using bias and flat-field correction procedures. We used DIA to extract high-precision time-series photometry in the field of NGC 3201. As in previous papers, we used the `DanDIA`[6] pipeline for the data reduction process (Bramich et al. 2013), which includes an algorithm that models the convolution kernel, matching the PSF of a pair of images of the same field as a discrete pixel array (Bramich 2008).

A brief summary of the `DanDIA` pipeline can be found, e.g., in the paper by Arellano Ferro et al. (2013a), while a detailed description of the procedure and its caveats are available in the paper by Bramich et al. (2011), to which the interested reader is referred for the relevant details.

We also used the methodology developed by Bramich & Freudling (2012) to solve for the magnitude offset that may be introduced into the photometry by the error in the fitted value of the photometric scale factor corresponding to each image. The magnitude

[6] `DanDIA` is built from the DanIDL library of IDL routines available at `http://www.danidl.co.uk/`.

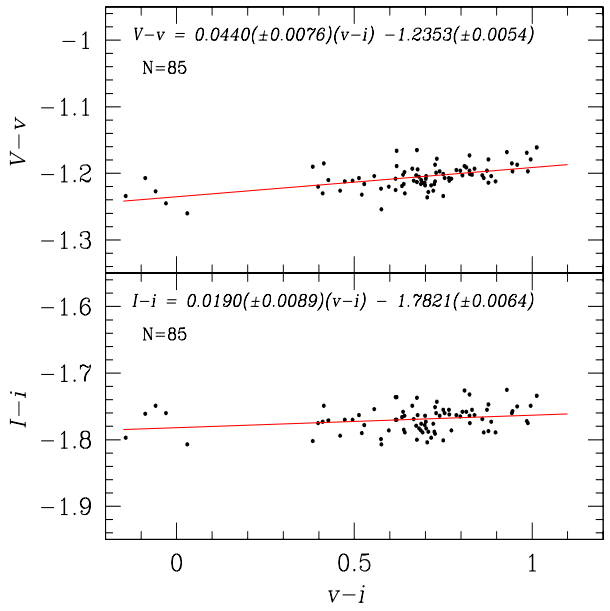

Fig. 1. The transformation relationship between the instrumental and standard photometric systems using a set of standards of Stetson (2000) in the FoV of our images of NGC 3201.

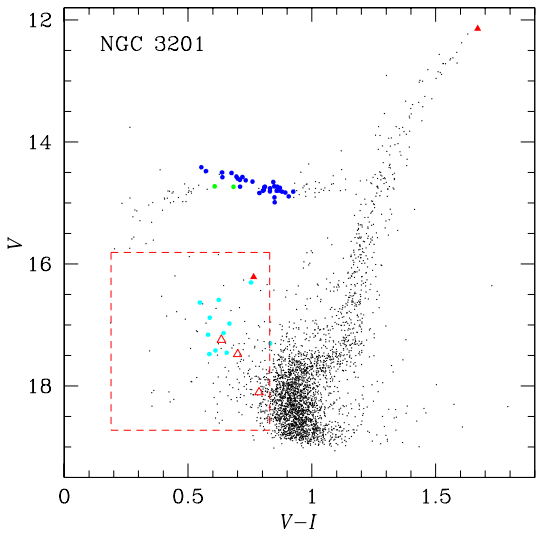

Fig. 2. CMD of NGC 3201. The magnitudes and colors plotted are magnitude-weighted means over our entire collection of images. Blue and green circles are, respectively, RRab and RRc variables in our FoV. An arbitrarily defined *blue straggler* region is enclosed by the dashed lines. Known SX Phe stars are represented by cyan circles. We searched for light variability in all stars inside that region and discovered three new SX Phe shown as red open triangles. The SR variable V117 and the eclipsing binary V119 are represented by solid red triangles.

offset due to this error can reach up to ≈30 mmag in a few cases, but it is generally of the order of ≈1−10 mmag. This correction improved the quality of the light curves, particularly for the brightest stars.

2.3. *Transformation to the VI standard system*

From the high number of standard stars of Stetson (2000)[7] in the large field of NGC 3201, 85 were identified in the FoV of our images with V and $V-I$ in the ranges 12.6–18.6 mag and −0.14–1.01 mag, respectively. These were used to transform our instrumental system into the Johnson-Kron-Cousins photometric system (Landolt 1992). The standard minus the instrumental magnitude differences show a mild dependence on the color as displayed in Figure 1. The transformation equations are of the form:

$$V = v + 0.0440\,(\pm 0.0076)\,(v-i) - 1.2353\,(\pm 0.0054), \quad (1)$$

$$I = i + 0.0190\,(\pm 0.0089)\,(v-i) - 1.7821\,(\pm 0.0064). \quad (2)$$

[7] http://www3.cadc-ccda.hia-iha.nrc-cnrc.gc.ca/community/STETSON/standards/.

3. VARIABLE STARS IN NGC 3201

The variable stars in our FoV are listed in Table 1 along with their mean magnitudes, amplitudes, and periods derived from our photometry. The coordinates listed in columns 10 and 11 are taken from the CVSGC, and were calculated by Samus et al. (2009) and Mazur et al. (2003). We found them to be accurate and no attempt to recalculate them was made. We include them here for the sake of completeness.

3.1. *The Color-Magnitude diagram*

The CMD of the cluster is shown in Figure 2, where the location of the known and the newly discovered variables is marked. Individual stars are discussed in the following section. The red-dashed area is an arbitrarily defined *blue straggler* region were SX Phe variables are expected to be found. Indeed, examination of the light curves of all stars in this region confirmed the nature of all previously known SX Phe stars and led to the discovery of three more (see § 3.3). The finding chart of all variables in Table 1 is in Figure 3. Given the differential nature of the reddening in front of the cluster we made no attempt to deredden the CMD. An interesting and successful exercise of this procedure may be found in LS03.

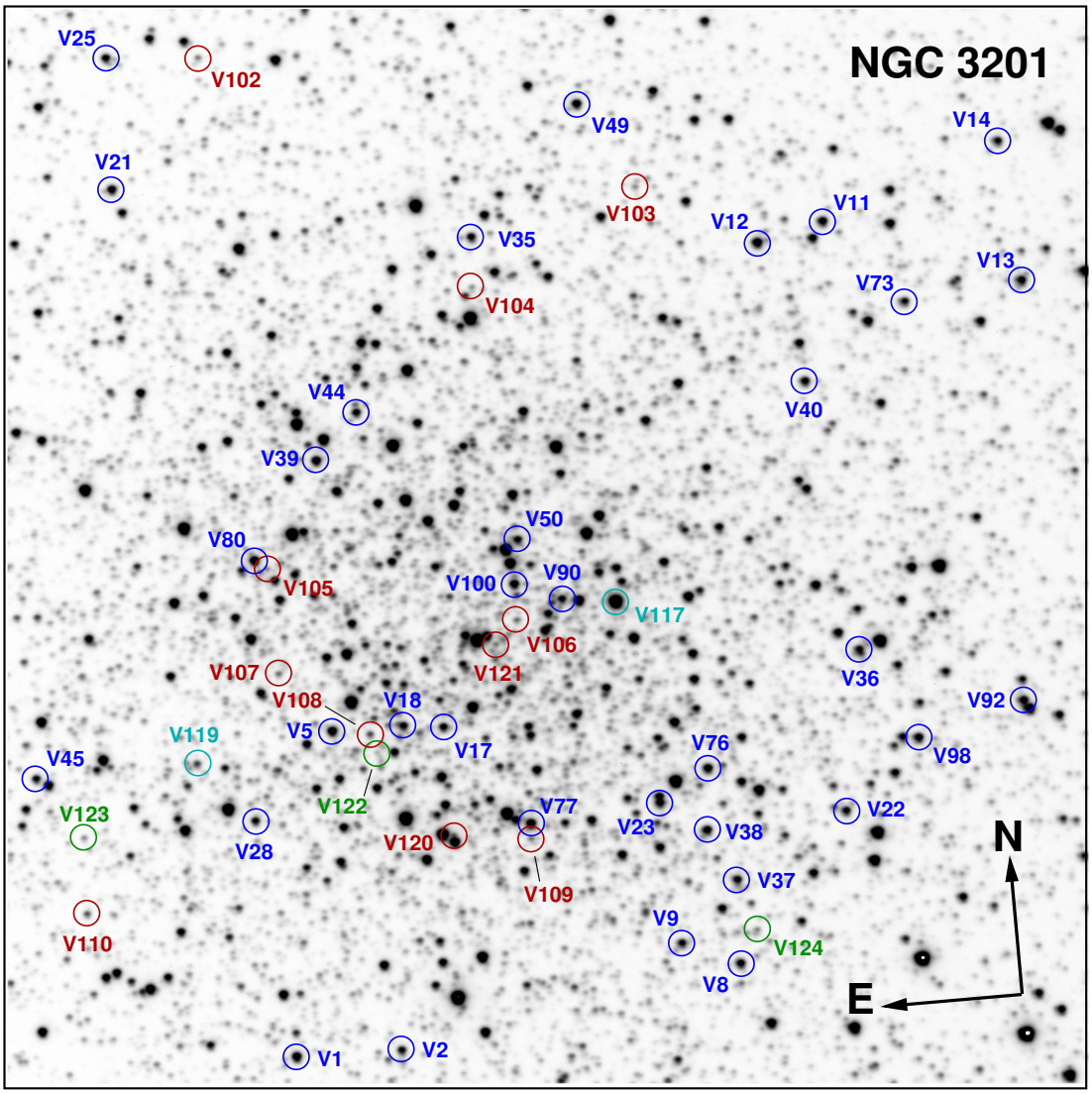

Fig. 3. Finding chart constructed from 9 of our best images in V. The field is about 5.1×5.1 arcmin^2. Labels are: blue for known RR Lyrae stars, red for known SX Phe stars, and green for the three SX Phe discovered in this work. The SR variable V117 and the eclipsing binary V119 are labeled in light blue.

3.2. *RR Lyrae stars*

A comparison of the intensity-weighted means $<V>$ and $<I>$ (Table 1) and those of LS03 for 27 RR Lyrae stars in common indicates that, on average, our $<V>$ values are 0.02 mag fainter and the $<I>$ values are 0.004 mag brighter, i.e., well within photometric errors. Therefore, the periods of the RR Lyrae stars were calculated by combining the V data from LS03 obtained in 1999 with our V photometry using the string-length method (Burke, et al. 1970; Dworetsky 1983). The 14 year time-base allows a precise determination of the periods. In Table 1 the new periods and epochs are listed, and for comparison the periods of LS03 are included as well. The V and I light curves of RRab and RRc stars are shown in Figures 4 and 6 respectively, having been phased by using our refined periods and the epochs listed in Table 1. In the light curves, observations from different nights are plotted with different colors for clarity; data from LS03 are also plotted in light gray. We can see that the LS03 light curves and ours match very well and are properly phased with the new periods. Later in this paper, when dealing with the Fourier decomposition, we shall exclusively use our data except in a few cases where data from LS03 nicely complete a light curve not properly covered otherwise, e.g., V14, V38, or V39. Plotting both data sets unveils long-term amplitude modulations of the Blazhko type not easily evident in our four-night light curves. These probable Blazhko variables, V18, V25, V28, V50, and V73 are labeled "Bl" or "Bl:" in Table 1.

3.3. *SX Phe stars*

Since our photometry spans only four nights and the seeing was not particularly good, we refrained

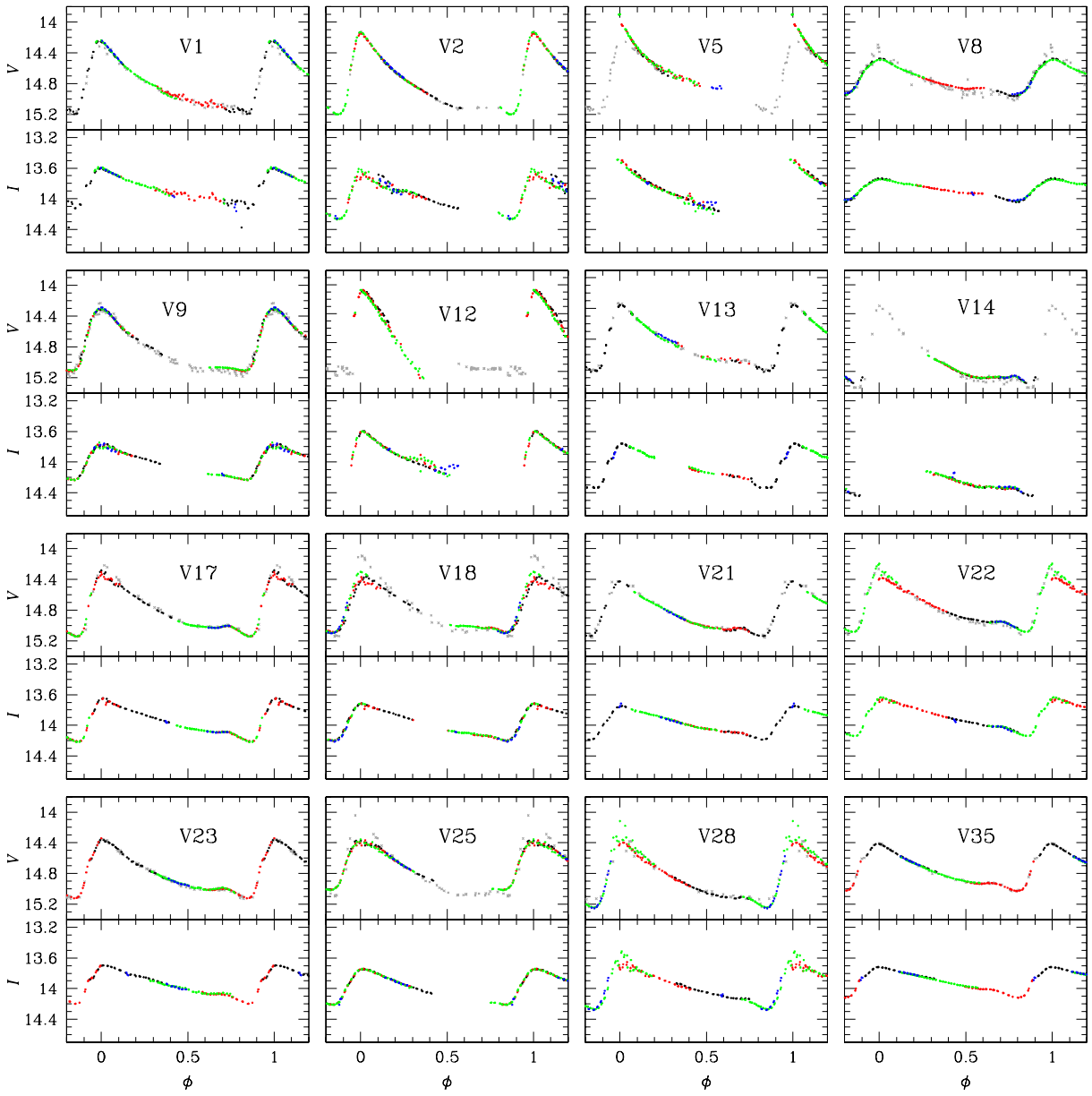

Fig. 4. Light curves of the RRab stars in our FoV phased with the periods listed in Table 1. The vertical scale is the same for all curves. The symbols in black, red, green, and blue correspond to each one of the four nights of our run, respectively. Gray symbols are data from LS03 and are included as a reference. See text for discussion on individual stars.

from performing the statistical approach we followed in previous papers (e.g., Arellano Ferro et al. 2013a,b; Figuera Jaimes et al. 2013) to identify new variable stars in our light curve collection. Instead, we examined the light curves of all stars lying on the blue straggler region shown in the CMD of Figure 2. This procedure allowed us to recover all known or suspected SX Phe stars in the CVSGC, as well as to find three new ones, which we labeled V122, V123, and V124. These stars will be discussed in detail later in this paper. The light curves of the 14 currently known SX Phe stars in the cluster are shown in Figure 5 and were phased with main periods calculated with period04 (Lenz & Breger 2005). The ephemerides and amplitudes of the main frequencies are listed in Table 1.

The appearance of many of the light curves strongly suggests the presence of multiple excited modes. In fact, as reported in the discovering paper (Mazur et al. 2003), several frequency modes can be identified in the majority of these SX Phe stars (see their Table 3) and therefore we were motivated to carry out an independent search of active modes in them. Although our photometry did not permit the detection of the many secondary frequencies reported by Mazur et al. (2003), we could confirm the principal frequencies and, in some stars, we were able to find secondary frequencies which

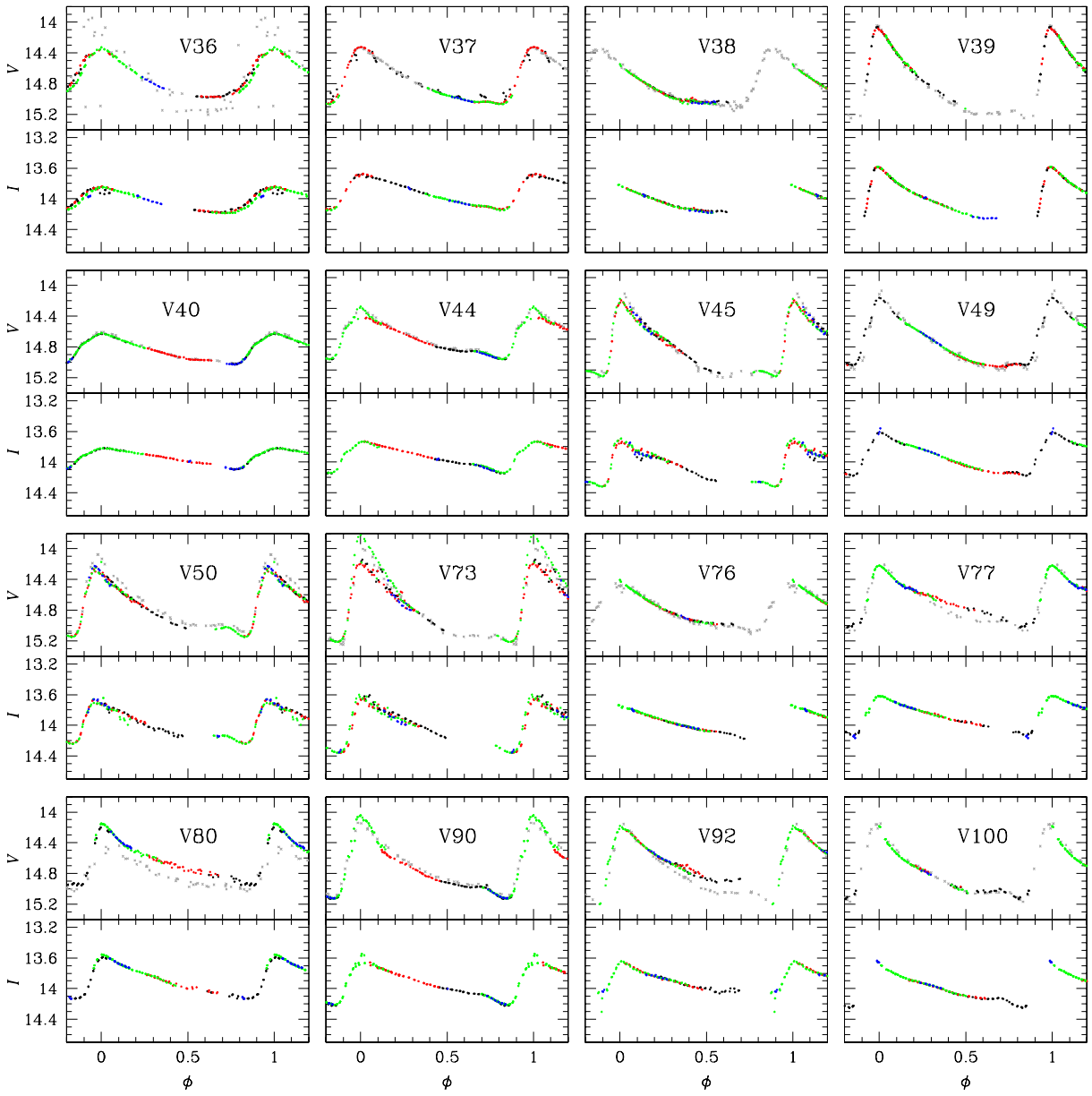

Fig. 4. Continued

led to the identification of the modes. Our frequency findings are given in Table 2.

Variables V120 and V121 are labeled as "SXP?" in the 2012 CVSGC. This classification comes most likely from Table 8 of LS03, where these stars (776 and 941 respectively) are labeled as "δ Scuti?". Given their frequencies in Table 2 and their position in the blue straggler region, we confirm the SX Phe character of both stars. We also performed a frequency analysis of the new SX Phe stars V122, V123, and V124. In stars V103, V106, and V108 two frequencies were detected and identified with the radial fundamental and first overtone modes, exhibiting ratios f_1/f_2 very close to the predicted value of 0.783 (see Santolamazza et al. 2001; Jeon et al. 2003; Poretti et al. 2005). One of the pulsating modes of V107 seems to be non-radial.

3.4. *Comments on individual variables*

In this section we only discuss those variable stars that deserve particular comments.

V5, V11, V12, V13, V39, V76, V77, V80, V98, V100. As mentioned before, in the reported observations the seeing appears to worsen along the night. This led to additional scatter in the light curves of these stars due to contamination by neighbouring stars, particularly near the minima. We thus either neglected them as much as possible or did not include them in the further analysis (e.g., stars V5 and V12).

V14. Our phase coverage for this light curve is incomplete, and as a result, our values of $<V>$ and $<I>$ are biased. We therefore used the values from LS03 to plot the star in the CMD and included LS03

TABLE 1

GENERAL DATA FOR THE CONFIRMED VARIABLES IN NGC 3201*

Variable Star ID	Variable Type	$< V >$ (mag)	$< I >$ (mag)	A_V (mag)	A_I (mag)	P (LS03) (d)	$\mathrm{HJD_{max}}$ (+2 450 000)	P (this work) (d)	RA (J2000.0)	Dec (J2000.0)
V1	RRab	14.841	13.887	0.951	0.560	0.6048761	6373.5087	0.604811(4)	10:17:42.82	−46:26:37.8
V2	RRab	14.839	14.002	1.081	0.653	0.5326722	6373.5922	0.532621(5)	10:17:39.98	−46:26:37.9
V5	RRab	–	–	1.231	–	0.511550	6373.4929	0.501345(4)	10:17:41.28	−46:25:06.3
V8	RRab	14.760	13.884	0.475	0.303	0.6286573	6371.7232	0.628568(5)	10:17:30.75	−46:26:19.3
V9	RRab	14.834	14.034	0.820	0.485	0.525530	6374.7383	0.525397(4)	10:17:32.28	−46:26:12.6
V11	RRc	14.808	14.136	0.49	0.312	0.299049	6373.5632	0.299134(3)	10:17:27.55	−46:22:55.6
V12	RRab	–	–	–	–	0.4955547	6373.5087	0.497369(4)	10:17:29.03	−46:22:55.8
V13	RRab	14.883	14.070	0.894	0.603	0.5752145	6371.7280	0.574822(5)	10:17:22.03	−46:23:11.2
V14	RRab	15.009	–	1.130	–	0.5092945	1216.7563	0.508941(5)	10:17:22.42	−46:22:31.5
V17	RRab	14.820	13.960	0.840	0.566	0.565590	6371.5406	0.565844(5)	10:17:38.29	−46:25:07.2
V18	RRab Bl:	14.812	13.983	0.732	0.494	0.539655	6373.7508	0.540442(5)	10:17:39.40	−46:25:07.0
V21	RRab	14.858	13.979	0.723	0.446	0.566628	6371.7429	0.566754(5)	10:17:46.23	−46:22:29.4
V22	RRab	14.753	13.897	0.833	0.503	0.6059882	6373.7086	0.605843(5)	10:17:27.64	−46:25:38.0
V23	RRab	14.818	13.951	0.771	0.501	0.586775	6372.7320	0.586776(5)	10:17:32.64	−46:25:31.1
V25	RRab Bl:	14.787	14.029	0.633	0.468	0.514804	6373.6127	0.514696(3)	10:17:46.15	−46:21:52.1
V28	RRab Bl:	14.885	13.981	0.981	0.57–0.77	0.580025	6373.6570	0.579506(5)	10:17:43.50	−46:25:30.4
V35	RRab	14.771	13.912	0.619	0.400	0.6155244	6371.5674	0.615523(5)	10:17:36.29	−46:22:43.2
V36	RRab	14.751	14.051	0.655	0.341	0.484178	6373.6570	0.479576(5)	10:17:27.01	−46:24:53.0
V37	RRab	14.785	13.932	0.746	0.476	0.575740	6372.6919	0.575145(4)	10:17:30.69	−46:25:55.7
V38	RRab	14.836	–	0.734	–	0.509090	6373.4900	0.509405(5)	10:17:31.42	−46:25:41.1
V39	RRab	14.879	–	1.244	–	0.483233	6373.4900	0.482872(5)	10:17:41.23	−46:23:49.7
V40	RRab	14.854	13.948	0.403	0.279	0.643820	6373.6100	0.643744(4)	10:17:28.00	−46:23:35.9
V44	RRab	14.803	13.933	0.687	0.411	0.6107344	6373.6991	0.610663(4)	10:17:40.08	−46:23:36.7
V45	RRab	14.974	14.089	1.002	0.629	0.537460	6373.6127	0.538058(4)	10:17:49.29	−46:25:14.6
V49	RRab	14.760	13.946	0.896	0.586	0.581020	6371.6775	0.580957(4)	10:17:33.63	−46:22:13.4
V50	RRab Bl:	14.832	14.020	0.916	0.582	0.542178	6373.6745	0.542347(5)	10:17:36.10	−46:24:14.0
V73	RRab Bl	14.816	14.061	1.06–1.38	0.740	0.519965	6373.5991	0.519538(5)	10:17:25.20	−46:23:15.2
V76	RRab	14.821	–	0.623	–	0.526680	6373.4900	0.526736(4)	10:17:31.29	−46:25:23.6
V77	RRab	14.693	13.891	1.079	0.529	0.567644	6373.5303	0.567393(7)	10:17:36.13	−46:25:36.1
V80	RRab	14.650	13.910	0.810	0.618	0.589960	6373.5108	0.588706(7)	10:17:43.07	−46:24:16.8
V90	RRab	14.753	13.935	1.081	0.58–0.66	0.606105	6373.6680	0.606387(6)	10:17:34.95	−46:24:33.3
V92	RRab	14.736	13.934	1.083	0.557	0.539585	6373.5534	0.539528(6)	10:17:22.70	−46:25:11.0
V98	RRc	14.759	14.053	0.38–0.46	0.243	0.335647	6373.5322	0.336259(5)	10:17:25.14	−46:25:20.0
V100	RRab	14.813	–	0.986	–	0.548920	6373.4900	0.548513(6)	10:17:36.14	−46:24:27.9
V102	SX Phe	17.164	16.574	0.060	–	–	6374.7421	0.045398(18)	10:17:43.50	−46:21:53.4
V103	SX Phe	17.424	16.804	0.054	–	–	6373.6570	0.037241(62)	10:17:32.10	−46:22:37.9
V104	SX Phe	17.457	16.800	0.038	–	–	6371.7233	0.037510(73)	10:17:36.60	−46:23:03.4
V105	SX Phe	17.506	16.894	0.060	–	–	6374.7621	0.037496(10)	10:17:42.60	−46:24:19.5
V106	SX Phe	16.883	16.291	0.034	–	–	6371.6818	0.043552(13)	10:17:36.00	−46:24:38.2
V107	SX Phe	16.982	16.307	0.126	–	–	6374.7503	0.040476(97)	10:17:42.50	−46:24:49.1
V108	SX Phe	16.325	15.551	0.236	–	–	6373.6897	0.067349(55)	10:17:40.20	−46:25:07.8
V109	SX Phe	17.176	16.498	0.302	–	–	6373.5394	0.054259(41)	10:17:36.00	−46:25:40.2
V110	SX Phe	16.603	15.965	0.249	–	–	6372.5672	0.050137(19)	10:17:48.10	−46:25:53.4
V117	SR	–	–	–	–	–	–	–	10:17:33.45	−46:24:34.6
V119	EA	16.218	15.45	0.04	0.04	–	6372.6511	1.2759	10:17:44.98	−46:25:13.3
V120	SX Phe	16.677	16.114	0.367	–	–	6372.6006	0.088162(46)	10:17:38.30	−46:25:38.0
V121	SX Phe	17.312	16.475	0.127	–	–	6373.5602	0.037369(18)	10:17:36.58	−46:24:43.2
V122[a]	SX Phe	18.107	17.324	0.053	–	–	6371.7700	0.067279(48)	10:17:40.15	−46:25:12.7
V123[a]	SX Phe	17.480	16.804	0.058	–	–	6374.7657	0.034895(8)	10:17:48.12	−46:25:32.2
V124[a]	SX Phe	17.245	16.607	0.022	–	–	6372.6720	0.040128(32)	10:17:30.22	−46:26:09.1

*In the FoV of our images. Previous period estimates for each variable from LS03 are reported in Column 7 for comparision with our refined periods in Column 9. The period uncertainties in parenthesis correspond to the last decimal places.

[a]Newly found in this work.

data to complete the light curve in order to perform Fourier decomposition.

V25 and V36. The shapes of the light curves of these stars are peculiar, showing very small amplitudes for their periods. In the case of V25, the addition of the LS03 light curve hints at the presence of amplitude modulations. For star V36, LS03 data are very scattered and do not follow our light curve. These stars will stand out as peculiar in the Bailey diagram discussed later (§ 4.1).

V117. The light curve of this star, which is the brightest of the cluster in our FoV, noticeably degraded after the post-calibration process described in § 2.2, which seems to have failed in this particular case. Hence, the light curve shown in Figure 7 was not post-calibrated. The intra-night variations are likely not real but originated from the seeing variations. The

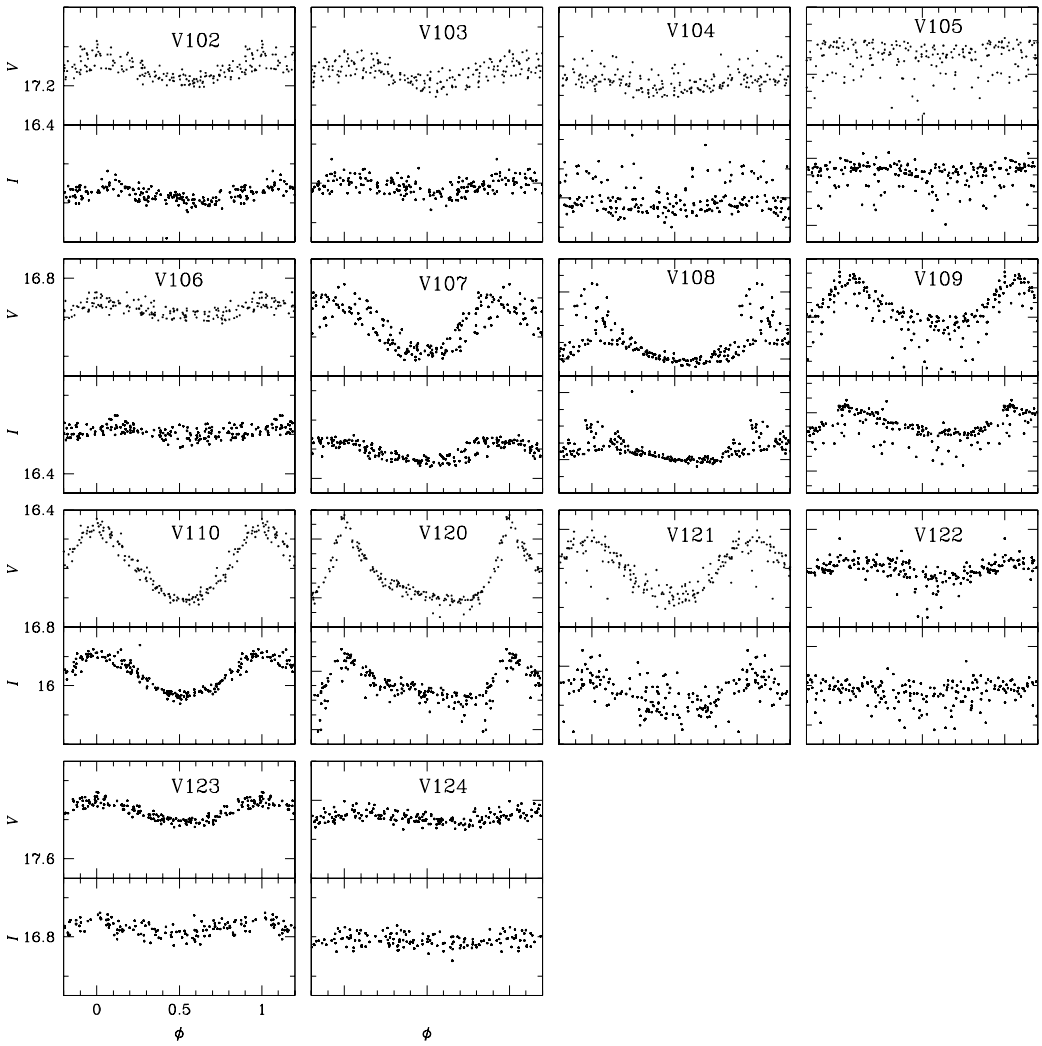

Fig. 5. Light curves of the SX Phe stars in our FoV phased with the main period listed in Table 1. The vertical scale is not the same for all curves; the tick mark on the vertical axis is equivalent to 0.1 mag. Variables V122, V123, and V124 are new discoveries.

real variation is reflected as a gradual dimming over the four nights.

V119. Figure 8 shows the light curve of this eclipsing binary phased with a period of 1.2759 days. With our data it is not possible to distinguish between this period and another of 0.595941 days.

4. PHYSICAL PARAMETERS OF RR LYRAE STARS

The shape of the light curve of an RR Lyrae star carries information of some of its physical parameters of astrophysical relevance such as [Fe/H], $\log(L/L_{\odot})$, and $\log T_{\rm eff}$. These can be calculated by means of the Fourier decomposition of the light curve, which is performed by fitting it with a series model of the form:

$$m(t) = A_0 + \sum_{k=1}^{N} A_k \cos\left(\frac{2\pi}{P}\ k\ (t-E) + \phi_k\right), \quad (3)$$

where $m(t)$ is the magnitude at time t, P is the period, and E is the epoch. A linear minimization routine is used to derive the best fit values of the amplitudes A_k and phases ϕ_k of the sinusoidal components. From the amplitudes and phases of the harmonics in equation 3, the Fourier parameters, defined as $\phi_{ij} = j\phi_i - i\phi_j$, and $R_{ij} = A_i/A_j$, are computed.

It has been shown that *ad hoc* semi-empirical calibrations can correlate the above Fourier parameters with the physical quantities of interest. Although numerous calibrations exist in the literature, in previous papers we have argued in favor of those developed by Jurcsik & Kovács (1996) and Kovács & Walker

TABLE 2

FREQUENCIES AND AMPLITUDES OF THE SX PHE STARS IN NGC 3201*

Variable	V	$V-I$	$E(B-V)$[a]	f (d^{-1})	A (mag)	P (d)	Mode id.[b]
V102	17.164	0.581	0.30	22.027	0.060	0.045398(18)	f_1:F
V103	17.423	0.611	0.23	26.852	0.054	0.037241(11)	f_1:F
				34.367	0.045	0.029097(8)	f_2:1O; f_1/f_2=0.781
V104	17.457	0.656	0.23	26.659	0.038	0.037510(43)	F
V105	17.506	0.586	0.23	26.670	0.060	0.037496(10)	F
V106	16.883	0.588	0.11	22.961	0.034	0.043552(13)	f_1:F
				29.240	0.023	0.034200(39)	f_2:1O; f_1/f_2=0.785
V107	16.982	0.667	0.23	24.706	0.126	0.040476(97)	f_1:F
				25.245	0.081	0.039610(33)	f_2:non-radial
V108	16.325	0.754	0.11	14.848	0.236	0.067349(55)	f_1:F
				19.073	0.122	0.052430(92)	f_2:1O; f_1/f_2=0.778
V109	17.176	0.643	0.29	18.430	0.302	0.054259(41)	f_1:F
V110	16.603	0.624	0.23	19.945	0.249	0.050137(19)	f_1:F
V120	16.677	0.548	0.33	11.342	0.367	0.088162(46)	f_1:F
V121	17.312	0.832	0.23	26.760	0.127	0.037369(18)	f_1:F
V122	18.107	0.787	–	14.863	0.053	0.067279(48)	f_1:F
V123	17.480	0.700	0.23	28.658	0.058	0.034895(8)	f_1:F
V124	17.245	0.634	0.23	24.920	0.022	0.040128(32)	f_1:F

*The numbers in parentheses indicate the uncertainty on the last decimal places.

[a]See § 5 for a discussion on the individual reddenings; [b]F: Fundamental mode; 1O: First overtone.

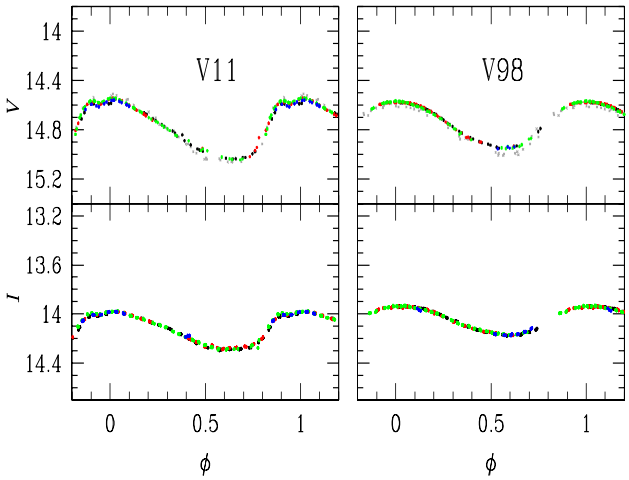

Fig. 6. Light curves of the two RRc stars in our FoV. Symbols are as in Figure 4.

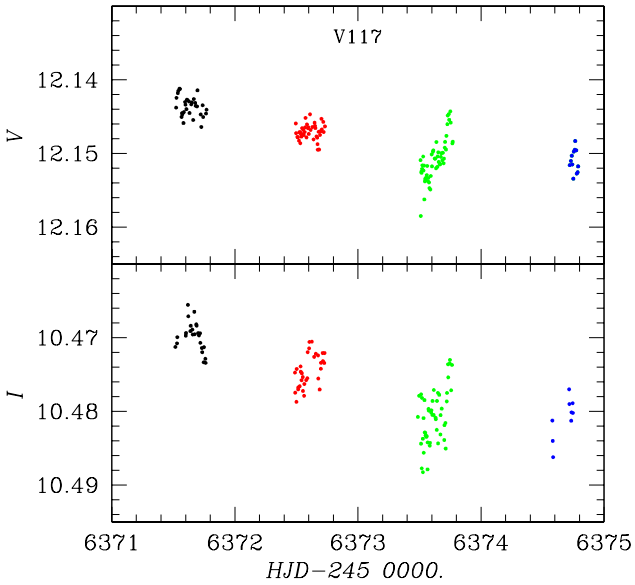

Fig. 7. V and I light curves of the SR variable V117. Intra-night variations are likely due to noise from seeing variations. The gradual fainting over the four nights should be real.

(2001) for the iron abundance and absolute magnitude of RRab stars, and those of Morgan, Wahl & Wieckhorts (2007) and Kovács (1998) for RRc stars. The effective temperature $T_{\rm eff}$ was estimated using the calibration of Jurcsik (1998). These calibrations and their zero points have been discussed in detail in Arellano Ferro et al. (2013a).

Due to the presence of differential reddening, before estimating the distance to the cluster from its

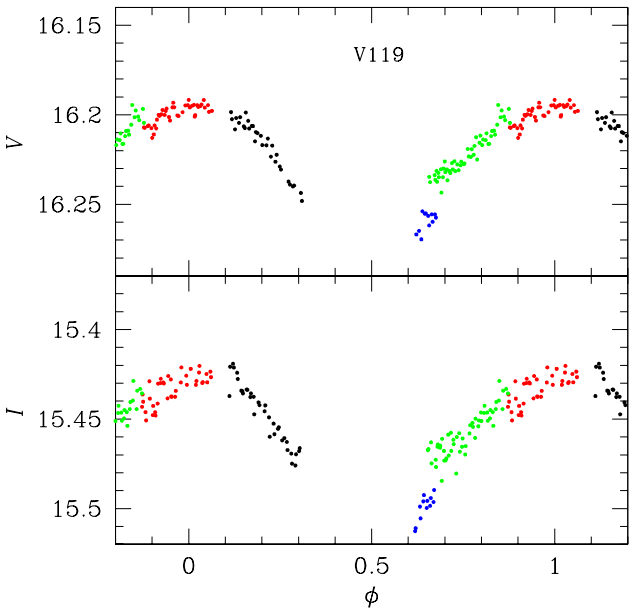

Fig. 8. V and I light curves of the eclipsing binary V119 phased with $P = 1.2759$ days.

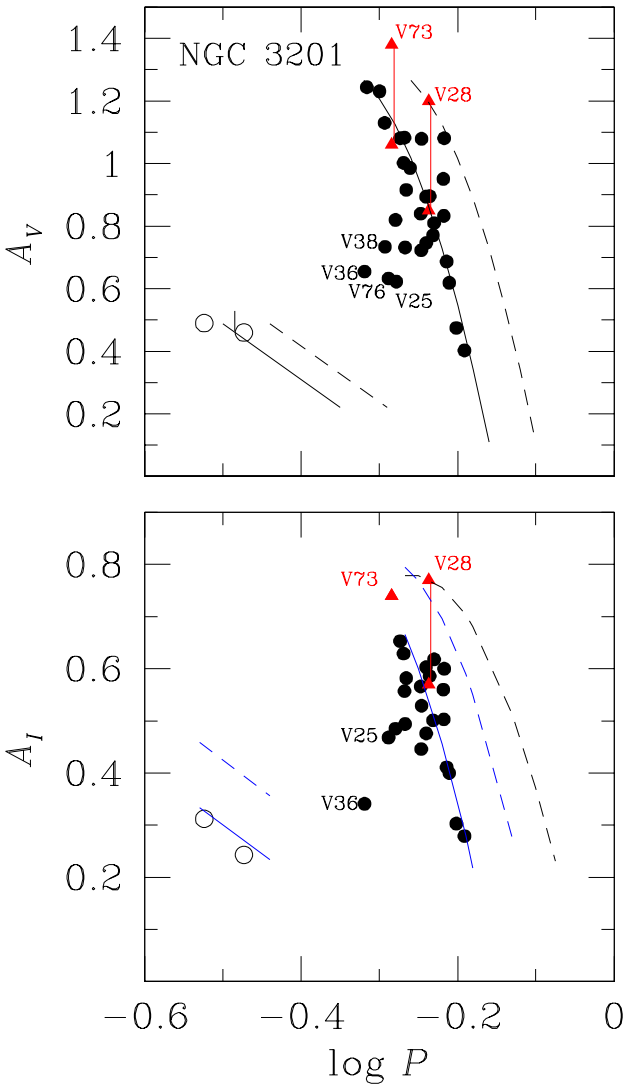

Fig. 9. Bailey diagram of NGC 3201 for V and I amplitudes. In the top panel the continuous and segmented lines are the loci found by Cacciari et al. (2005) in the OoI cluster M3. In the bottom panel the black segmented locus was found by Arellano Ferro et al. (2011, 2013a) for the OoII clusters NGC 5024 and NGC 6333. The blue loci are from Kunder et al. (2013). See § 4.1 for details.

RR Lyrae stars it is necessary to individually correct their magnitudes. We estimated the individual color excesses using the method originally proposed by Sturch (1966), and further investigated by Blanco (1992), Mateo et al. (1995), and Guldenschuh et al. (2005). Guldenschuh et al. (2005) concluded that, for RRab stars, the intrinsic color between phases 0.5 and 0.8 is $(V-I)_0^{\phi(0.5-0.8)} = 0.58 \pm 0.02$ mag. We have already successfully applied this method to the RR Lyrae stars of another cluster with heavy differential reddening, NGC 6333 (Arellano Ferro et al. 2013a). In the case of the present work, however, we noted that in several of the RRab light curves in Figure 4 the bump appears in phases smaller than 0.8, so we restricted the calculation of <V> and <I> to the 0.5–0.7 range. Then we calculated $E(B-V) = E(V-I)/1.616$. The resulting reddenings for the RRab stars are listed in Column 10 of Table 3. Values of $E(B-V)$ for stars with scant or peculiar data in the above phase range (e.g., V50, V77, and V80) are marked with a colon, and for them we adopted instead the mean reddening value in subsequent calculations. The same approach was followed by LS03 and their values are listed in their Table 6. A comparison of both sets of reddenings for the 14 stars in common reveals that, with a scatter of 0.03 mag, our values are on average 0.03 mag smaller. The average of our reddenings is 0.23 ± 0.02, which compares well with the value 0.25 ± 0.02 of LS03 for stars within 2 arcmin of the cluster center.

The value of A_0 and the Fourier light-curve fitting parameters for 24 RRab and 2 RRc stars with no apparent signs of amplitude modulations (see Figure 4) are listed in Table 3. These Fourier parameters and the above mentioned calibrations were used in turn to calculate the physical parameters listed in Table 4. The absolute magnitude M_V was converted into luminosity with $\log(L/L_\odot) = -0.4\,(M_V - M_{\rm bol} + BC)$. The bolometric correction was calculated using the formula $BC = 0.06\,[{\rm Fe/H}]_{ZW} + 0.06$ given by Sandage & Cacciari (1990). We adopted $M_{\rm bol}^\odot = 4.75$ mag.

Before the iron calibration of Jurcsik & Kovács (1996) for RRab stars can be applied to the light curves, a "compatibility condition parameter" D_m should be calculated. For the definition of D_m see

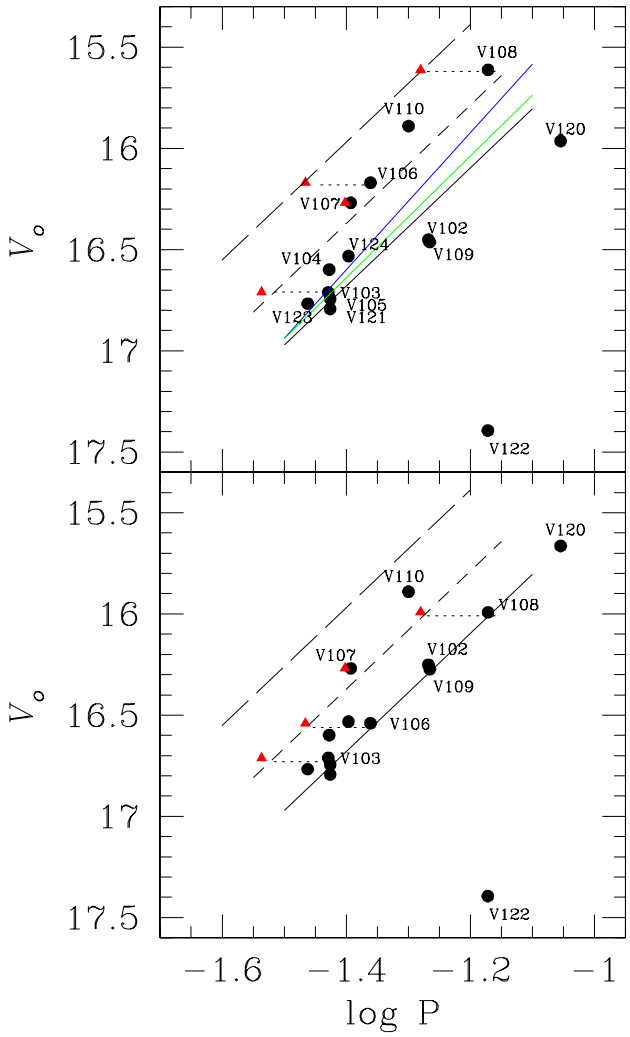

Fig. 10. Period-Luminosity (P-L) relation for SX Phe stars. In the top panel the black lines correspond to the fundamental mode P-L calibration of Arellano Ferro et al. (2011) for the SX Phe in NGC 5024, and their corresponding first and second overtone loci, all shifted to the distance of 5.0 kpc obtained from the RR Lyrae stars. The blue and green lines are the fundamental mode calibrations of Cohen & Sarajedini (2012) and Jeon et al. (2003). All these loci were also shifted to the distance of 5.0 kpc. Magnitudes and loci have been dereddened by $E(B-V) = 0.23$. The scatter shown by the star distribution is mostly due to differential reddening. In the bottom panel we modified the individual reddenings to reconcile the double-mode pulsators V108 and V109 with the fundamental and first overtone loci. Also small shifts were applied to V102, V109, and V120. Stars V107 and V110 were not moved. Star V107 has an active non-radial mode, while the position of V110 may indicate that it pulsates either in the first overtone or that its reddening is smaller. Variable V122 is likely not a cluster member. Stars V124, V104, V105, V123, and V121, in order of increasing brightness, are not labeled in the bottom panel. See § 5 for a discussion.

the works of Jurcsik & Kovács (1996) and Kovács & Kanbur (1998). These authors advise to consider only light curves for which $D_m < 3.0$. The values of D_m for each of the RR Lyrae stars are also listed in Table 3. Most of them fulfill the D_m criterion and, in order to maintain the size of our sample reasonable, we did not exclude stars V1–V14, which have values marginally larger than 3.0. This practice has been followed by some previous authors (e.g. Arellano Ferro et al. 2013a; Kains et al. 2013; Cacciari et al. 2005). Stars V25 and V36 show large uncertainties in their Fourier coefficients as well as large values of D_m, so they were not considered in the calculation of physical quantities.

The resulting physical parameters of the RR Lyrae stars are summarized in Table 4. The mean values given in the bottom of the table are weighted by the statistical uncertainties. Also listed are the corresponding distances. Given the period, luminosity, and temperature for each RR Lyrae star, its mass and radius can be estimated from the equations: $\log M/M_\odot = 16.907 - 1.47 \log P_F + 1.24 \log (L/L_\odot) - 5.12 \log T_{\rm eff}$ (van Albada & Baker 1971), and $L{=}4\pi R^2 \sigma T^4$ respectively. The masses and radii given in Table 4 are expressed in solar units.

4.1. *Bailey diagram and Oosterhoff type*

The Bailey diagram is a plot of the period versus the amplitude for RR Lyrae stars; it offers insight on the Oosterhoff type of a globular cluster and helps to identify possible peculiar amplitude stars for a given period. The Bailey diagram of M3 is usually used as a reference for OoI clusters (see Figure 4 of Cacciari et al. 2005). Figure 9 displays the corresponding distribution of the RR Lyrae stars in NGC 3201 with a good light curve coverage. The continuous and segmented lines in the top diagram represent, respectively, the mean distributions of non-evolved and evolved stars in M3 according to Cacciari et al. (2005). In recent papers we compared these loci with the distributions of RR Lyrae stars in the OoII clusters NGC 5024 (Arellano Ferro et al. 2011, Figure 7), NGC 6333 (Arellano Ferro et al. 2013a, Figure 17), and NGC 7099 (Kains et al. 2013, Figure 10). We, like Cacciari et al. (2005), found that the A_V amplitudes of RRab stars follow the loci of the candidate evolved stars in M3, i.e., the segmented line. As for the RRc stars, however, we differ from Cacciari et al. (2005) in that the distributions in the OoII clusters NGC 5024 and NGC 6333 do not follow the defined trend in M3 RRc stars but are rather scattered, and that their distribution is altered by the presence of Blazhko-like amplitude modulations, particularly in the case of NGC 5024 (Arellano Ferro et al. 2012). It is clear from this figure that the RRab and RRc stars in NGC 3201 follow the trend found in M3, which identifies NGC 3201 as being of the type OoI. In Arellano Ferro et al. (2011) the distribution of

TABLE 3

FOURIER COEFFICIENTS OF RRab AND RRc STARS IN NGC 3201*

Variable ID	A_0 (V mag)	A_1 (V mag)	A_2 (V mag)	A_3 (V mag)	A_4 (V mag)	ϕ_{21}	ϕ_{31}	ϕ_{41}	$E(B-V)$	N	D_m
RRab											
V1	14.841(2)	0.331(2)	0.171(2)	0.106(2)	0.065(2)	4.030(19)	8.277(30)	6.204(45)	0.301	7	5.2
V2	14.839(2)	0.357(3)	0.171(2)	0.144(2)	0.083(2)	3.721(18)	7.906(24)	5.951(36)	0.247	10	3.1
V8	14.760(1)	0.173(1)	0.085(1)	0.049(1)	0.017(1)	3.962(19)	8.474(29)	6.645(72)	0.214	9	7.6
V9	14.834(2)	0.318(3)	0.092(3)	0.030(3)	0.016(2)	3.864(28)	8.122(46)	5.872(67)	0.201	7	3.8
V13	14.883(4)	0.296(2)	0.148(2)	0.109(2)	0.063(2)	3.953(21)	8.285(31)	6.302(43)	0.186	9	4.9
V14	15.009(3)	0.400(4)	0.186(4)	0.134(5)	0.095(3)	3.761(33)	7.910(47)	5.824(74)	0.223	9	5.4
V17	14.820(2)	0.291(3)	0.132(3)	0.095(3)	0.064(2)	3.918(26)	8.262(37)	6.433(54)	0.224	7	1.4
V21	14.858(1)	0.267(1)	0.115(1)	0.080(1)	0.047(1)	3.991(11)	8.374(17)	6.484(26)	0.239	7	1.2
V23	14.818(1)	0.268(2)	0.132(2)	0.091(2)	0.055(2)	4.012(17)	8.283(25)	6.478(37)	0.222	7	1.3
V25	14.787(5)	0.278(4)	0.107(5)	0.062(4)	0.033(6)	3.882(55)	8.179(137)	6.289(260)	–	10	12.1
V35	14.771(1)	0.228(1)	0.104(1)	0.065(1)	0.034(1)	4.068(15)	8.482(23)	6.980(39)	0.215	7	1.2
V36	14.751(4)	0.280(6)	0.093(6)	0.037(5)	0.016(5)	3.712(52)	7.773(139)	5.102(312)	–	8	9.4
V37	14.785(1)	0.312(1)	0.121(1)	0.067(1)	0.039(1)	4.063(9)	8.353(14)	6.392(24)	0.228	7	2.2
V38	14.836(1)	0.303(2)	0.133(2)	0.077(2)	0.039(2)	3.818(18)	8.068(30)	5.963(52)	0.18:	9	1.6
V39	14.879(2)	0.430(3)	0.193(3)	0.150(3)	0.101(3)	3.804(20)	7.899(27)	5.839(36)	0.228	9	1.0
V40	14.854(1)	0.162(1)	0.060(1)	0.033(1)	0.012(1)	4.182(19)	8.611(31)	7.287(68)	0.235	5	2.7
V45	14.974(3)	0.372(5)	0.140(5)	0.115(5)	0.081(5)	3.915(43)	8.095(57)	5.952(81)	0.249	10	2.6
V49	14.760(1)	0.355(2)	0.139(2)	0.090(2)	0.058(2)	4.049(16)	8.180(24)	5.978(36)	0.213	7	2.3
V50	14.832(2)	0.318(4)	0.135(3)	0.104(3)	0.076(4)	3.841(34)	8.018(46)	6.025(62)	0.18:	10	1.0
V76	14.821(2)	0.249(3)	0.112(3)	0.058(3)	0.029(3)	3.964(31)	8.427(54)	6.828(80)	0.200	8	1.9
V77	14.693(2)	0.254(2)	0.153(2)	0.097(2)	0.052(3)	4.490(23)	9.115(37)	7.200(60)	0.19:	8	2.5
V80	14.650(2)	0.241(3)	0.137(3)	0.101(2)	0.063(3)	4.187(27)	8.539(39)	6.626(55)	0.17:	8	2.3
V90	14.753(2)	0.332(4)	0.191(4)	0.139(4)	0.085(4)	3.986(30)	8.153(44)	5.986(65)	0.213	9	2.5
V100	14.813(2)	0.324(3)	0.152(2)	0.128(2)	0.078(2)	3.911(23)	7.999(29)	5.886(43)	0.210	9	1.9
RRc											
V11	14.802(1)	0.235(2)	0.060(2)	0.027(2)	0.015(2)	4.589(40)	3.111(77)	1.891(158)	0.23	4	
V98	14.759(2)	0.191(1)	0.018(1)	0.010(1)	0.001(1)	4.826(102)	3.711(187)	4.653(742)	0.23	4	

*The numbers in parentheses indicate the uncertainty on the last decimal place. Also listed are the number of harmonics N used to fit the light curve of each variable and the deviation parameter D_m.

A_I amplitudes in the OoII cluster NGC 5024 was also defined and is shown as a black segmented line in the bottom panel of Figure 9. It follows the equation:

$$A_I = (-0.313 \pm 0.112) - (8.467 \pm 1.193) \log P - (16.404 \pm 0.441) \log P^2. \quad (4)$$

Also in the bottom panel of Figure 9 the distribution of the I amplitudes of RRab and RRc stars in NGC 3201 is shown. The blue loci are those calculated by Kunder et al. (2013) for the OoI clusters for the RRab and RRc stars (solid lines) and for the OoII clusters (segmented lines). Their OoI locus represents well the distribution in NGC 3201. We note the difference between the locus of OoII clusters proposed by Kunder et al. (2013) and the one observed by Arellano Ferro et al. (2011, 2013a) in NGC 5402 and NGC 6333 respectively.

5. SX PHE STARS: THE PERIOD-LUMINOSITY RELATION

The Period-Luminosity relation for SX Phe stars (PLSX) has recently been calibrated by several authors, notably Poretti et al. (2008) and McNamara (1997) for Galactic and extragalactic δ Scuti and SX Phe stars. In globular clusters the PLSX has been studied by Jeon et al. (2003) and Arellano Ferro et al. (2011) for NGC 5024, and McNamara (2000) for ω Cen. The calibrations of Arellano Ferro et al. (2011) for the fundamental mode of SX Phe stars in NGC 5024 in the V and I filters are of the form:

$$M_V = -2.916 \log P - 0.898, \quad (5)$$

and

$$M_I = -2.892 \log P - 1.072. \quad (6)$$

TABLE 4

PHYSICAL PARAMETERS OF THE RRab AND RRc STARS*

Star	[Fe/H]$_{ZW}$	M_V	log $T_{\rm eff}$	log($L/L_\odot$)	D (kpc)	$M/M_\odot$	$R/R_\odot$
			RRab				
V1	−1.589(28)	0.523(3)	3.806(9)	1.691(1)	4.75	0.69(7)	5.66(1)
V2	−1.665(23)	0.628(4)	3.809(8)	1.649(2)	4.89	0.71(7)	5.25(1)
V8	−1.487(25)	0.627(1)	3.800(10)	1.649(1)	4.94	0.62(8)	5.34(1)
V9	−1.436(43)	0.590(4)	3.814(10)	1.664(2)	5.30	0.71(9)	4.81(2)
V13	−1.468(29)	0.608(3)	3.808(8)	1.657(1)	5.40	0.66(7)	5.064(1)
V14	−1.572(44)	0.607(6)	3.815(11)	1.657(2)	5.52	0.73(9)	5.115(2)
V17	−1.452(35)	0.616(4)	3.808(9)	1.653(2)	5.03	0.67(7)	5.01(1)
V21	−1.348(16)	0.631(1)	3.809(7)	1.647(1)	4.98	0.65(6)	5.02(1)
V23	−1.511(23)	0.610(3)	3.805(8)	1.656(1)	5.06	0.66(6)	5.12(1)
V35	−1.435(22)	0.595(1)	3.801(8)	1.662(1)	5.03	0.66(6)	5.27(1)
V37	−1.419(13)	0.549(1)	3.809(7)	1.680(1)	5.08	0.69(6)	5.09(1)
V38	−1.425(28)	0.672(3)	3.814(9)	1.631(1)	4.93	0.68(7)	4.72(2)
V39	−1.484(25)	0.628(4)	3.818(8)	1.649(2)	5.11	0.73(7)	4.58(1)
V40	−1.422(29)	0.608(1)	3.796(10)	1.657(1)	5.05	0.64(8)	5.41(1)
V45	−1.504(54)	0.580(7)	3.813(11)	1.668(3)	5.30	0.70(9)	4.87(2)
V49	−1.595(23)	0.513(3)	3.809(8)	1.695(1)	5.22	0.71(7)	5.53(1)
V50	−1.594(43)	0.627(5)	3.809(10)	1.649(2)	5.02	0.69(8)	5.30(2)
V76	−1.153(51)[a]	0.692(4)	3.812(11)	1.623(2)	5.03	0.65(9)	4.81(2)
V77	−0.660(35)[a]	0.657(3)	3.820(10)	1.637(1)	4.65	0.55(6)	5.03(1)
V80	−1.282(37)[a]	0.646(4)	3.808(9)	1.642(2)	4.58	0.61(7)	5.14(2)
V90	−1.711(41)	0.547(6)	3.805(10)	1.681(2)	5.12	0.68(8)	5.66(2)
V100	−1.638(27)	0.629(4)	3.809(8)	1.648(2)	5.09	0.68(7)	5.34(1)
Weighted mean	−1.483(6)	0.604(1)	3.808(2)	1.658(1)	5.00	0.67(2)	5.12(1)
σ	±0.098	±0.045	±0.005	±0.016	±0.22	±0.03	±0.25
			RRc				
V11	−1.46(14)	0.574(2)	3.868(1)	1.670(1)	5.04	0.57(1)	4.15(4)
V98	−1.55(37)	0.590(4)	3.864(1)	1.664(2)	4.91	0.50(1)	4.78(12)
Weighted mean	−1.47(12)	0.576(1)	3.867(1)	1.667(2)	5.03	0.56(1)	4.21(4)
σ	±0.06	±0.011	±0.003	±0.016	±0.09	±0.05	±0.45

*The numbers in parentheses indicate the uncertainty on the last decimal place. Also listed are the number of harmonics N used to fit the light curve of each variable and the deviation parameter D_m.

[a]Value not considered in the average.

These calibrations have been used to calculate the distance to globular clusters with SX Phe stars independently of their RR Lyrae population (e.g., Arellano Ferro et al. 2013a,b).

In the top panel of Figure 10 the distribution of the SX Phe stars is shown in the log $P-V_0$ plane. To deredden them we adopted the mean reddening estimated for the RR Lyrae stars in § 3.2, $E(B-V) = 0.23$. The continuous line corresponds to the calibration for the fundamental mode of equation 5 scaled to the distance of 5.0 kpc, obtained from the 22 RRab stars in Table 4 (see § 4).

The dotted and dashed lines correspond to the loci of the first and second overtones assuming the ratios 0.783 and 0.571 (see Santolamazza et al. 2001; Jeon et al. 2003; Poretti et al. 2005). It is clear that the distribution of SX Phe stars shows scatter, which is most likely due to differential reddening. However, we note that the group around V103 matches the fundamental mode rather well. It is also worth paying attention to the position of the three double-mode stars V103, V106, and V108, for which we also plotted the first overtone period with red triangles. In these stars we detected the fundamental and first overtone frequencies, identified as such from their ratio (§ 3.3). To reconcile the positions of the stars with the pulsation loci, one may assume a slightly different reddening for each star. In this way we obtained the bottom panel of Figure 10, and the procedure was as follows. The two double-mode stars V106 and V108 were shifted to the fundamental mode line by modifying their reddening

TABLE 5

TIME-SERIES V AND I PHOTOMETRY FOR CONFIRMED VARIABLES IN OUR FIELD OF VIEW*

Variable Star ID	Filter	HJD (d)	$M_{\rm std}$ (mag)	$m_{\rm ins}$ (mag)	σ_m (mag)	$f_{\rm ref}$ (ADU s^{-1})	$\sigma_{\rm ref}$ (ADU s^{-1})	$f_{\rm diff}$ (ADU s^{-1})	$\sigma_{\rm diff}$ (ADU s^{-1})	p
V1	V	2456371.52286	15.126	16.348	0.001	6014.959	4.635	−3115.105	3.956	0.9966
V1	V	2456371.52599	15.137	16.359	0.001	6014.959	4.635	−3157.769	3.334	1.0006
⋮	⋮	⋮	⋮	⋮	⋮	⋮	⋮	⋮	⋮	
V1	I	2456371.51722	14.053	15.830	0.002	6831.708	7.004	−2176.444	9.449	1.0030
V1	I	2456371.51972	14.017	15.793	0.002	6831.708	7.004	−2018.446	9.645	1.0047
⋮	⋮	⋮	⋮	⋮	⋮	⋮	⋮	⋮	⋮	
V2	V	2456371.52286	14.457	15.685	0.001	2795.928	4.714	+2514.549	4.843	0.996
V2	V	2456371.52598	14.477	15.706	0.001	2795.928	4.714	+2424.449	3.992	1.0006
⋮	⋮	⋮	⋮	⋮	⋮	⋮	⋮	⋮	⋮	
V2	I	2456371.51722	13.687	15.466	0.002	4060.533	7.058	+2464.694	11.144	1.0030
V2	I	2456371.51972	13.799	15.578	0.002	4060.533	7.058	+1827.676	11.074	1.0047
⋮	⋮	⋮	⋮	⋮	⋮	⋮	⋮	⋮	⋮	

*The standard $M_{\rm std}$ and instrumental $m_{\rm ins}$ magnitudes are listed in columns 4 and 5, respectively, corresponding to the variable stars in column 1. Filter and epoch of mid-exposure are listed in columns 2 and 3, respectively. The uncertainty on $m_{\rm ins}$ is listed in column 6, which also corresponds to the uncertainty on $M_{\rm std}$. For completeness, we also list the reference and differential fluxes $f_{\rm dref}$ and $f_{\rm diff}$ and the scale factor p in columns 7, 9, and 11, along with the uncertainties $\sigma_{\rm ref}$ and $\sigma_{\rm diff}$ in columns 8 and 10. This is a representative extract from the full table, which is available at the CDS.

to $E(B-V) = 0.11$ in both cases. Note that the corresponding first overtone mode, represented by the red triangles, also matches well the first overtone locus for these double-mode stars. Small reddening adjustments were also applied to stars V102, V109, and V120. The estimated reddening values for all SX Phe stars are listed in the 4th column of Table 2. Star V122 is much too faint for its period, and an unacceptably large value of the reddening would be required to bring it to the fundamental locus. For these reasons, we believe that this SX Phe star is not a cluster member.

We note at this point that the slopes of the V and I P–L relations for NGC 3201 seem consistent with those observed in NGC 5024 (Arellano Ferro et al. 2011) and also with the V slopes observed in NGC 5024 by Jeon et al. (2003) (green line in Figure 10) and in NGC 288 (Arellano Ferro et al. 2013b). The slope found by Cohen & Sarajedini (2012) for the fundamental mode is a little steeper (blue line in Figure 10). Both Jeon et al.'s (2003) and Cohen & Sarajedini's (2012) calibrations are consistent with our distance determination of 5.0 kpc; however, if these calibrations are preferred, the individual reddenings of the SX Phe discussed above would have to be slightly modified.

We may conclude that the SX Phe stars indicate a distance to the cluster consistent with that derived by the Fourier decomposition of the RRab stars, i.e., 5.0 kpc, and that by invoking adequate values for the differential reddening of these stars it can be argued that their main frequency corresponds to the fundamental mode, and that V103, V106, and V108 are double-mode radial pulsators.

6. SUMMARY OF RESULTS

We have presented the results of the Fourier decomposition of RR Lyrae stars and the frequency analysis of SX Phe stars in the central parts of the globular cluster NGC 3201, based on difference image analysis of a CCD time-series.

The differential reddening of the cluster was addressed and individual reddenings for the RRab stars were estimated from $V-I$ curves using the method outlined and calibrated most recently by Guldenschuh et al. (2005). We found an average $E(B-V) = 0.23\pm0.02$ from a sample of 18 RRab stars with adequate phase coverage. In the calculation of the distance, however, we used the individual reddenings.

Iron abundance and distance were calculated from the light curve Fourier decomposition of 22 RRab and 2 RRc stars contained in the FoV of our images without obvious signs of amplitude modulation. We found, for the RRab stars, a mean iron abundance $[{\rm Fe/H}]_{ZW} = -1.483 \pm 0.090$ (systematic uncertainty) and a mean distance of 5.00 ± 0.22 kpc (systematic). For the RRc stars the results were, respectively: $[{\rm Fe/H}]_{ZW} = -1.47 \pm 0.06$ and 5.03 ± 0.09 kpc (both are also systematic uncertainties). Since these results come from independent calibrations for the RRab and

RRc stars, they can be considered as two independent determinations of metallicity and distance. The iron abundance in the scale of Carretta et al. (2009), transformed using the equation:

$$[\mathrm{Fe/H}]_{\mathrm{UVES}} = -0.413 + 0.130\,[\mathrm{Fe/H}]_{ZW} - 0.356\,[\mathrm{Fe/H}]^2_{ZW}, \quad (7)$$

is $[\mathrm{Fe/H}]_{\mathrm{UVES}} = -1.39 \pm 0.13$. To the best of our knowledge no previous estimates of [Fe/H] from Fourier decomposition of the RR Lyrae light curves exist for this cluster. Other estimates of [Fe/H] include: -1.54 ± 0.16 and -1.89 ± 0.16 calculated by LS03 from their $B-V$ and $V-I$ CMDs, -1.53 ± 0.03 (Rutledge et al. 1997), and -1.61 ± 0.12 (Zinn & West 1984). Within the uncertainties, our metallicity $[\mathrm{Fe/H}]_{ZW} = -1.483 \pm 0.090$ is in good concordance with these published values.

The calculation of the cluster distance by LS03 was made via the globular cluster M_V and [Fe/H] correlation (e.g., Chaboyer 1999) for RR Lyrae stars, and yielded 4.87 ± 0.27 kpc for [Fe/H]$= -1.53$. This is in good agreement with the result of our RR Lyrae Fourier decomposition. LS03 also calculated the cluster distance based on two SX Phe stars, #752 and #1019 (in their numbering) which, judging from their mean magnitudes and periods, very likely correspond to variables V110 and V109, respectively. They used the PLSX calibration of Petersen & Hog (1998) and derived a distance of 4.67 ± 0.24 kpc. Our own calculation is based on a larger number of SX Phe, a more complete mode identification for most of them, some assumptions on the differential reddening, and the use of a different P-L calibration (see § 5). It was shown that, in the P-L distribution of SX Phe stars, both the fundamental and the first overtone modes loci are consistent with the average distance 5.00 ± 0.23 kpc found from the RR Lyrae stars.

Finally, we discovered three new SX Phe stars, numbered V122, V123, and V124. Very likely, star V122 is not a cluster member but a background object. Three clear radial double-mode SX Phe stars have been identified, i.e., V103, V106, and V108. Star V107 seems to be a double-mode star with a non-radial component.

APPENDIX A

Our V and I photometry for all variable stars in the FoV of our images is only available in electronic form. Here, in Table 5, we show only a portion of it for guidance regarding its form and content.

We warmly thank Dr. Daniel Bramich for allowing us the use `DanDIA` and for guiding our reduction process, as well as for useful and opportune comments. We are thankful to our referee Christine Clement for her constructive suggestions and comments. AAF acknowledges Roberto Figuera Jaimes for his valuable help in the first stages of the data reduction. We are indebted to the CONACyT (México) and MINCyT (Argentina) for financial support through the interchange project 188769 (MX/12/09). AAF acknowledges the support from DGAPA-UNAM grant through project IN104612, and is thankful to the European Southern Observatory (Garching), and to the Observatorio Astronómico of the Universidad Nacional de Córdoba (Argentina) for warm hospitality during different stages of this work. We have made an extensive use of the SIMBAD and ADS services, for which we are thankful.

REFERENCES

Arellano Ferro, A., Bramich, D.M., Figuera Jaimes, R., et al. 2013a, MNRAS, 434, 1220
Arellano Ferro, A., Bramich, D. M., Figuera Jaimes, R., Giridhar, S., & Kuppuswamy, K. 2012, MNRAS, 420, 1333
Arellano Ferro, A., Bramich, D.M., Giridhar, S., et al. 2013b, AcA, 63, 429
Arellano Ferro, A., Figuera Jaimes, R., Giridhar, Sunetra, Bramich, D. M., Hernández Santisteban, J. V., & Kuppuswamy, K. 2011, MNRAS, 416, 2265
Bailey, S.I. 1922, Harvard Circ., 234, 1
Blanco, V. M. 1992, AJ, 104, 734
Bramich D. M. 2008, MNRAS, 386, L77
Bramich, D. M., Horne, K., Albrow, M. D., et al. 2013, MNRAS, 428, 2275
Bramich, D. M., Figuera, R., Giridhar, S., Arellano Ferro, A. 2011, MNRAS, 413, 1275
Bramich, D.M., & Freudling, W. 2012, MNRAS, 424, 1584
Burke, E. W., Rolland, W. W., & Boy, W. R. 1970, Journal of the Royal Astronomical Society of Canada, 64, 353
Cacciari, C., Corwin, T. M., & Carney, B. W. 2005, AJ, 129, 267
Carretta, E., Bragaglia, A., Gratton, R., D'Orazi, V., & Lucatello, S. 2009, A&A, 508, 695
Clement, C. M., et al. 2001, AJ, 122, 2587.
Cohen, R. E., & Sarajedini, A. 2012, MNRAS, 419, 342
Chaboyer, B. 1999, in Post-Hipparcos cosmic candles, ed. A. Heck & F. Caputo (Dordrecht: Kluwer), p. 111
Dowse, M. 1940, Harvard Bull., 913, 17
Dworetsky, M. M. 1983, MNRAS, 203, 917
Figuera Jaimes, R., Arellano Ferro, A., Bramich, D. M., Giridhar, S., & Kuppuswamy, K., 2013, A&A, 556, A20
Guldenschuh, K. A., Layden, A. C., Wan, Y., et al. 2005, PASP, 117, 721
Jeon, Y.-B., Lee M. G., Kim S.-L, & Lee H. 2003, AJ, 125, 3165
Jurcsik, J. 1998, A&A, 333, 571
Jurcsik, J., & Kovács G. 1996, A&A, 312, 111
Kains, N., Bramich, D. M., Arellano Ferro A., et al. 2013, A&A, 555, 36
Kains N., Bramich D. M., Figuera Jaimes R., Arellano Ferro A., Giridhar S., & Kuppuswamy K. 2012, A&A, 548, 92
Kovács, G. 1998, Mem. Soc. Astron. Ital., 69, 49
Kovács, G., & Kanbur S.M. 1998, MNRAS, 295, 834
Kovács, G., & Walker, A.R. 2001, A&A, 371, 579
Kunder, A., Stetson, P.B., Catelan, M., Walker, A.R., & Amigo, P. 2013, AJ, 145, 33

Landolt, A. U. 1992, AJ, 104, 340
Layden, A.C., & Sarajedini, A. 2003, AJ, 125, 208 (LS03)
Lenz, P., & Breger M. 2005, Communications in Asteroseismology, 146, 53
Lee, S.-W. 1977, A&A Supp., 28, 409
McNamara D. H. 1997, PASP, 109, 1221
_____. 2000, PASP, 112, 1096
Mateo, M., Udalski, A., Szymanski, M., Kaluzny, J., Kubiak, M., & Krzeminski, W. 1995, AJ, 109, 588
Mazur, B., Krzemiński, W., & Thompson, I. B. 2003, MNRAS, 340, 1205
Morgan, S. M., Wahl, J. N., & Wieckhorst, R. M. 2007, MNRAS, 374, 1421
Petersen, J.O., & Hog, E. 1998, A&A, 331, 989
Piotto, G., King, I.R., Djorgovski, S. G. et al. 2002 A&A, 391, 945
Poretti, E., Clementini, G., Held, E. V. et al. 2008, ApJ, 685, 947
Poretti, E., Suárez, J. C., Niarchos, P. G. et al. 2005, A&A, 440, 1097
Rutledge, G. A., Hesser, J. E., & Stetson, P. B. 1997, PASP, 109, 907
Samus, N. N., Kazarovets, E. V., Pastukhova, E. N., Tsvetkova, T. M., & Durlevich, O. V. 2009, PASP, 121, 1378
Sandage, A., & Cacciari, C. 1990, ApJ, 350, 645
Santolamazza, P., Marconi, M., Bono, G., Caputo, F., Cassisi, S., & Gilliland, R.L. 2001, ApJ, 554, 1124.
Stetson, P.B. 2000, PASP, 112, 925
Sturch, C. 1966, ApJ, 143, 774
van Albada, T. S., & Baker, N. 1971, ApJ, 169, 311
von Braun, K., & Mateo, M. 2001, AJ, 113, 264
_____. 2002, AJ, 123, 279
Wilkens, H. 1965, Asociación Argentina de Astronomía, Bols. 8,9 & 10, 66
Woods, I. E. 1919, Harvard Circ., 216, 1
Wright, F. W. 1941, Harvard Bull., 915, 2
Zinn, R., West, M. J. 1984, ApJS, 55, 45

J. A. Ahumada and J. H. Calderón: Observatorio Astronómico, Universidad Nacional de Córdoba, Laprida 854, 5000 Córdoba, Argentina (javier@oac.uncor.edu, jehumcal@gmail.com).
A. Arellano Ferro: Instituto de Astronomía, Universidad Nacional Autónoma de México, Apdo. Postal 70-264, México, D. F., C.P. 04510, Mexico (armando@astro.unam.mx).
N. Kains: Space Telescope Science Institute, 3700 San Martin Drive, Baltimore, MD 21218, USA (nkains@stsci.edu).